Theory of Saturation and Double Resonance Effects in ESR Spectra. III. rf Coherence and Line Shapes

JACK H. FREED* AND DANIEL S. LENIART
Department of Chemistry,† Cornell University, Ithaca, New York
AND
JAMES S. HYDE
Analytical Instrument Division, Varian Associates, Palo Alto, California

(Received 2 June 1967)

The theory of saturation in the electron spin resonance spectra of dilute solutions of free radicals has been employed to analyze in detail several possible effects in ENDOR spectra that are due to the coherent nature of the applied nuclear rf and microwave fields. These effects are implicitly contained in a "coherence matrix," although their observation also depends on the details of the relaxation terms. It is shown that (1) strong nuclear rf fields can split ESR lines, a phenomenon similar to "spin-tickling" in NMR double resonance, (2) strong microwave fields in the presence of weaker, but saturating, nuclear rf fields can split ENDOR lines, and this latter effect is demonstrated experimentally. A subtle coherence effect requiring nuclear spins of $I>\frac{1}{2}$, or more than one equivalent spin of $I=\frac{1}{2}$, and dependent upon nuclear rf field strength is carefully analyzed. It is predicted to significantly affect only the ENDOR line obtained from saturating the $M=0$ hyperfine line for two or four equivalent protons. The theory for this effect appears to be in very good agreement with detailed experimental studies on Coppinger's radical. Other radicals are also found to exhibit such coherence effects. The ability to distinguish and analyze them is deemed important in applying ENDOR as an analytical tool. Computer simulations of the line shapes in the presence of coherence effects are also presented.

I. INTRODUCTION

In several recently reported experiments,[1,2] the electron–nuclear double resonance (ENDOR) technique has been applied to free radicals in liquids with considerable success. This technique is of interest both as an analytical tool in simplifying complex hyperfine spectra of organic free radicals and also as a means for obtaining information on spin relaxation mechanisms of free radicals.

A detailed theoretical analysis of steady-state ENDOR effects in liquids also has recently been developed.[3,4] It predicts the strong dependence of an ENDOR signal upon the relative magnitudes of lattice-induced electronic and nuclear spin transitions. The theory was shown to predict, at least semiquantitatively,[4] many of the observations made in the initial experiments.[1,2] From a comparison of the theory with the experiments, it appears that the intramolecular electron–nuclear dipolar (END) interaction is the major contributer to the lattice-induced nuclear spin transitions when conditions are appropriate for large proton ENDOR enhancements. In the theoretical analysis, the role of the NMR field as inducing rapid nuclear-spin transitions (which could "short-out" the lattice-induced nuclear-spin transitions provided that the field strength is large enough) was stressed, although this is not the only effect of the NMR field.

In the first experimental paper on ENDOR of free radicals in liquids[1a] a splitting of the line from the four ring protons was observed, and it was argued that this indicated that the two pairs of ring protons were slightly inequivalent. Subsequent experiments mentioned briefly in an earlier publication[2] and reported fully here show that this interpretation was incorrect; the splitting disappears as the nuclear rf field is reduced. Moreover, in a complicated ENDOR study[2] involving overlapping ENDOR lines, changes in the shape of lines with nuclear rf power increased the difficulty of analysis.

In general, double-resonance experiments in which both the irradiated and observed transitions have one energy level in common exhibit a variety of coherence effects. Only a preliminary analysis of these phenomena was given in I. A major purpose of the present paper is to develop further the analysis of the effects on observed ENDOR spectra that are due to the coherent nature of the applied nuclear rf and microwave fields. It is important to account for such observed effects in order for the ENDOR technique to be useful as an analytical tool. The formulation developed here is compared with a variety of new experiments, and it appears that theory and experiment are in satisfactory agreement.

In Sec. II, the general theory is reviewed and particular attention is given to the formulation of the coherence or **K** matrix. In Sec. III several coherence effects involving a spin system with only a coupled electron spin and nuclear spin of $I=\frac{1}{2}$ are enumerated. One such effect is peculiar to the ENDOR situation and it serves to illustrate the procedures of the general treatment. In Sec. IV a new coherence effect involving a spin system with a nuclear spin of $I=1$ (or two equivalent spins of $I=\frac{1}{2}$) or higher and also peculiar to the ENDOR situation is examined in detail. By use

* Alfred P. Sloan Foundation Fellow.
† Supported in part by National Institutes of Health Grant No. GM 14123, and by the Advanced Research Projects Agency.
[1] (a) J. S. Hyde and A. H. Maki, J. Chem. Phys. **40**, 3117 (1964); (b) J. S. Hyde, *ibid.* **43**, 1806 (1965); (c) J. S. Hyde, R. Breslow, and C. DeBoer, J. Am. Chem. Soc. **88**, 4763 (1966).
[2] J. S. Hyde, J. Phys. Chem. **71**, 68 (1967).
[3] J. H. Freed, J. Chem. Phys. **43**, 2313 (1965). References to this work are designated by I.
[4] J. H. Freed, J. Phys. Chem. **71**, 38 (1967).

of the word "peculiar" we mean that these are *coherence* effects which manifest themselves when the double resonance signal arises from a change in *saturation* of the observed signal because of the presence of the irradiating field. In Sec. V the experiments are discussed in the light of the theory, and the conclusions are in Sec. VI.

II. REVIEW OF GENERAL THEORY

We start with the density-matrix equation of motion

$$\dot{\sigma}=-i[\mathcal{H}_0+\epsilon(t),\sigma]-\Gamma(\sigma-\sigma_0), \tag{2.1}$$

where $\mathcal{H}_0$ is the time-independent Hamiltonian:

$$\mathcal{H}_0=\gamma_e B_0 S_z-\sum_i \gamma_i B_0 I_{zi}-\gamma_e \sum_i \bar{a}_i S_z I_{zi}, \tag{2.1'}$$

from which transition frequencies are obtained, $\epsilon(t)$ is the interaction of the spins with the radiation fields and $\Gamma(\sigma-\sigma_0)$ contains the relaxation effects.[3] Equation (2.1) is valid for temperatures characteristic of normal liquids and when:

$$|\gamma_e B_0|, |\gamma_i B_0|, |\gamma_e \bar{a}_i|, \tau_c^{-1} \gg |\epsilon(t)|, |\Gamma(\sigma-\sigma_0)|, \tag{2.2}$$

where τ_c is a correlation time for the motional narrowing.[3] It was shown in the earlier papers[3,4] that for steady-state, multiple-resonance ESR experiments, Eq. (2.1) [subject to Eq. (2.2)] may be expressed in matrix form:

$$(\mathbf{K}+i\mathbf{R})\mathbf{Z}=\mathbf{D}\chi+\mathbf{Q}, \tag{2.3a}$$

and

$$\mathbf{W}^j\chi=-2\mathbf{D}^{trj}\mathbf{Z}'', \tag{2.3b}$$

with the solution:

$$\mathbf{Z}''=\mathbf{M}^{-1}(-\mathbf{R}^{-1})\mathbf{Q}, \tag{2.4a}$$

$$\mathbf{Z}'=(-\mathbf{R}^{-1})\mathbf{K}\mathbf{Z}'', \tag{2.4b}$$

$$\mathbf{M}=\mathbf{1}+(\mathbf{R}^{-1}\mathbf{K})^2+(-\mathbf{R}^{-1})\mathbf{S}. \tag{2.4c}$$

Here $\mathbf{Z}$ is a column vector with real and imaginary parts:

$$\mathbf{Z}=\mathbf{Z}'+i\mathbf{Z}''. \tag{2.3c}$$

Each component of $\mathbf{Z}'$ and $\mathbf{Z}''$ corresponds, respectively, to an absorption and a dispersion mode of a particular spin transition which is excited as a result of the applied rf fields. It is important for our present purposes to specify the directionality of the spin transitions. Thus for the simple case of a single electron spin interacting with a radiation field rotating at frequency ω and of strength B_1 we have[3]:

$$\epsilon(t)=\tfrac{1}{2}\gamma_e B_1(S_+e^{-i\omega t}+S_-e^{+i\omega t}). \tag{2.5}$$

Then we find a steady-state solution:

$$\sigma_{-,+}=\langle m_s=-|\,\sigma\,|\,m_s=+\rangle=Z_{-,+}e^{i\omega t}, \tag{2.6}$$

where $Z_{-,+}$ is constant in time, i.e., $\sigma_{-,+}$ is constant in the coordinate frame rotating at frequency ω. Now $Z''_{-,+}$ may be given physical meaning as being proportional to the *net* radiation induced absorption *from* State $m_s=-$ to State $m_s=+$, since it obeys [c.f., Eq. (2.3a) and I]:

$$Z''_{-,+}=d_e(\sigma_--\sigma_+)[T_2/(1+\Delta\omega_e^2T_2^2)], \tag{2.7}$$

where

$$\Delta\omega_e=\omega-\hbar^{-1}(E_+-E_-)=\omega-\omega_{+,-}, \tag{2.8}$$

T_2 is the transverse relaxation time for the electron spin, and $(\sigma_--\sigma_+)$ gives the steady-state *net population excess* in State $-$ over State $+$. That is, by *net* absorption is meant the induced transition rate from State $-$ to $+$ from which is subtracted the transition rate from State $+$ to $-$. It follows then, from this interpretation that

$$Z''_{+,-}=-Z''_{-,+}, \tag{2.9}$$

where $Z''_{+,-}$ is the *net* absorption from State $+$ to $-$. Equation (2.9) is easily shown to be a consequence of the Hermitian property of σ; relationships like it are useful for obtaining a physical understanding of the results. Now Eqs. (2.3) and (2.4) are valid for the convention that $\mathbf{Z}$ spans the space of all induced transitions in which there is (are) increase(s) in spin quantum number but *no* decrease(s) in spin quantum number. We refer to this as the raising convention.[5] It is sometimes impossible to describe all multiple-quantum effects by such a single convention, so that a more complex form of Eqs. (2.3) and (2.4) could become necessary. However, the examples treated in this paper are readily calculated utilizing the raising convention.

Returning to Eqs. (2.3) and (2.4), we note that the coherence matrix $\mathbf{K}$ which determines the resonant frequencies, the linewidth matrix $-\mathbf{R}$, and the saturation matrix $\mathbf{S}$ are all defined in the vector space of the induced transitions (i.e., the vector space spanned by $\mathbf{Z}''$). $\mathbf{Q}$ is a vector in this space. Now χ is a vector in the space defined by all the spin eigenstates. Thus the αth element represents the deviation from equilibrium population in the αth state:

$$\chi_\alpha=(\sigma_\alpha-\sigma_{0\alpha}). \tag{2.10}$$

Also $\mathbf{W}$, the transition probability matrix, is defined in this space of eigenstates, while $\mathbf{D}$ transforms $\mathbf{W}$ into the space of induced transitions according to

$$\mathbf{S}=2\mathbf{D}(W^j)^{-1}\mathbf{D}^{trj}. \tag{2.11}$$

The matrix $\mathbf{D}$ is composed of transition moments (see below). Methods for determining the $\mathbf{S}$ and $\mathbf{R}$ matrices are discussed in detail elsewhere.[3,4,6] We are presently concerned with the $\mathbf{K}$ matrix which yields the resonant frequencies and can be affected by the coherent nature of the radiation. The diagonal elements of $\mathbf{K}$ are ob-

[5] If a *lowering* convention were adopted, then $\mathbf{R}\rightarrow-\mathbf{R}$ in Eq. (2.3a), while the minus sign in Eq. (2.3b) should be dropped. Then the left-hand side in both Eqs. (2.4a) and (2.4b) must be multiplied by -1.

[6] J. H. Freed and G. K. Fraenkel, J. Chem. Phys. **39**, 326 (1963).

tained from:

$$-(\dot{\sigma}+i[\mathcal{H}_0, \sigma])\rightarrow K^{(d)}. \quad (2.12a)$$

The only nonvanishing terms are for $\sigma_{\alpha\beta}$, where $E_\alpha \neq E_\beta$ and $\alpha \leftrightarrow \beta$ is an induced transition. The nondiagonal elements of **K** are obtained from:

$$[\epsilon(t), \sigma]\rightarrow K^{(n)}, \quad (2.12b)$$

where only those terms involving $\sigma_{\alpha\beta}$, ($E_\alpha \neq E_\beta$ and $\alpha \leftrightarrow \beta$ an induced transition) are retained. [The terms diagonal in σ in Eq. (2.12b) lead to $\mathbf{D}\chi+\mathbf{Q}$ in Eq. (2.3a)].

When two rotating rf fields are present, where one at frequency ω_e lies close enough to a (degenerate) ESR transition to excite it, while the other at frequency ω_n is close to a (degenerate) NMR transition, we may generalize Eq. (2.5) to[7]

$$\epsilon(t) = \tfrac{1}{2}\gamma_e B_1[S_+ \exp(-i\omega_e t) + S_- \exp(+i\omega_e t)]$$
$$+\tfrac{1}{2}\gamma_r B_n[J_{r+} \exp(-i\omega_n t) + J_{r-} \exp(+i\omega_n t)]. \quad (2.13)$$

where the subscript r refers to that particular set of equivalent nuclear spins of resonant frequency ω_r such that $|\omega_n-\omega_r| = \Delta\omega_r \approx 0$. Note that

$$J_r = \sum_{i \text{ in } r} I_i, \quad (2.13')$$

where the sum is over the individual equivalent spins. We also define

$$\tfrac{1}{2}\gamma_e B_1 S_{-\lambda_j} \equiv d_{\lambda_j}, \quad (2.14a)$$

where d_{λ_j} is the "transition moment" for the λ_jth ESR transition and $S_{-\lambda_j}$ is the matrix element between the pair of spin states making up this transition. (Note that λ_j refers to the jth degenerate transition at frequency ω_λ). In a similar manner we define NMR transition moments

$$d_{\eta_j} \equiv \tfrac{1}{2}\gamma_r B_n J_{r-\eta_j}. \quad (2.14b)$$

It is now not difficult to develop a set of rules for the construction of **K** utilizing a diagram method.

Diagram Method for Elements of the K Matrix

An energy-level diagram such as the one in Fig. 1 for $S=\frac{1}{2}$ and $I=1$ is constructed. (In this example, ω_e is close to ω_{ab} and ω_n is close to $\omega_{bd}=\omega_{df}$.)

(1) Let an arrow be drawn between each pair of states for which the energy difference $\hbar\omega_{\lambda_j}$ is nearly resonant with an applied radiation field and for which a transition moment d_{λ_j} given by Eqs. (2.14) exists. Each arrow should point to the state of increasing spin quantum number. An arrow represents a single quantum transition corresponding to a steady-state, nonzero value for Z''_{λ_j}, where λ_j fulfills the raising convention, (e.g., in Fig. 1, they are $Z''_{ba} \equiv Z''_{fe}$; $Z''_{db} \equiv Z''_1$; $Z''_{fd} \equiv Z''_2$).

(2) Now consider all pairs of levels connected by two contiguous arrows (e.g., a and d, also b and f in Fig. 1). These lead to two quantum transitions, with which is associated a nonvanishing Z_{λ_j} (e.g., Z_{da} and $Z_{fb} \equiv Z_c$ in Fig. 1). The pairs of levels connected by three contiguous arrows are the triple quantum transitions (e.g., Z_{fa}), etc.

(3) The diagonal elements of **K** associated with the n-tuple quantum transitions are obtained by adding the $\Delta\omega_{\lambda_j}$ for the n consecutive single quantum transitions [e.g., $(\omega_n-\omega_{bd})+(\omega_n-\omega_{df})$ for Z_{fb}].

(4) The only off-diagonal elements of **K** for the n-tuple transitions are with $n-1$-tuple transitions and with $n+1$-tuple transitions, such that the $n\pm1$ tuple transition plus or minus a single quantum transition η_k equals the n-tuple transition. The matrix element is just $\pm d_{\eta_k}$, where the plus (minus) sign is used when the arrow for the η_kth transition points toward (away from) the state in common with the other constituent transition (either an $n-1$ or an n-tuple transition). (e.g., $K_{ba,da}=+d_n$; $K_{db,da}=-d_e$; $K_{da,fa}=+d_n$).

(5) The K matrix is symmetric in the vector space of the induced transitions.

As a result of the fact that there are no nonvanishing transition moments of type Eq. (2.14) between pairs of states coupled by multiple quantum transitions, there are no elements of **S** or **Q** involving such transitions. However, there are linewidths associated with multiple quantum transitions, and the formulas given in I and Refs. 4 and 6 for the **R** matrix are general enough to permit their calculation.

III. COHERENCE EFFECTS FROM STRONG ESR AND NMR FIELDS; $I=\frac{1}{2}$

The $I=\frac{1}{2}$ case was treated in I, but only the exactly resonant situation, when $\Delta_e=\Delta_n=0$, was discussed in detail. It was then possible to obtain a set of sufficiency conditions for the neglect of coherence effects in the

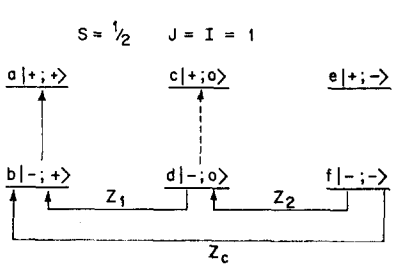

FIG. 1. Transitions and eigenstates for double resonance in a radical with $S=\frac{1}{2}$ and a nuclear spin of $I=1$ (or the $J=1$ states of two equivalent nuclear spins).

[7] Equation (2.13) is incomplete, since we have truncated all terms that do not make a direct resonant contribution. However, there is a singificant effect from $\frac{1}{2}\gamma_e B_n[S_+\exp(-i\omega_n t)+S_-\exp(+i\omega_n t)]$ on the calculation of d_r. See Footnote 34 in I for further details.

region close to resonance. They are[8]

$$1+d_e^2\Omega_e T_e \gg d_n^2 T_x T_e \tag{3.1}$$

for the coherence effect tending to split Z''_e into two components to be unimportant;

$$1+d_n^2\Omega_n T_n \gg d_e^2 T_x T_n \tag{3.2}$$

for the coherence effect tending to split Z''_n into two components to be unimportant; and further for

$$|\,\Omega_{e,n}\,| \gg T_x \tag{3.3}$$

in order that the enhancement term does not involve the coherent coupling between states a and b'. Here the T^{-1}'s are the linewidths (for Lorentzian line shapes) and the Ω's are the saturation parameters with the subscripts e, n, and x referring to the electron spin, nuclear spin, and double quantum transitions, as illustrated in Fig. 2. When $d_e \sim d_n$ and both are of saturating strength it should not be difficult to achieve these conditions.[3] We are presently concerned with examining the region where these coherence effects do become important, and learning in detail how they affect the line shapes which may be monitored. Utilizing the basic equations in I and Eqs. (2.4), we have for the present case, where ω_e and ω_n are close to $\omega_{aa'}$ and $\omega_{a'b'}$, respectively:

$$\mathbf{M}=\begin{pmatrix} 1+T_e^2\Delta_e^2+T_e(T_x d_n^2+\Omega_e d_e^2) & T_e d_e d_n(\Omega_{e,n}-T_x) & T_e d_n[T_e\Delta_e+T_x(\Delta_e+\Delta_n)] \\ T_n d_e d_n(\Omega_{e,n}-T_x) & 1+T_n^2\Delta_n^2+T_n(T_x d_e^2+\Omega_n d_n^2) & -T_n d_e[T_n\Delta_n+T_x(\Delta_e+\Delta_n)] \\ T_x d_n[T_e\Delta_e+T_x(\Delta_e+\Delta_n)] & -T_x d_e[T_n\Delta_n+T_x(\Delta_e+\Delta_n)] & 1+T_x^2(\Delta_e+\Delta_n)^2+T_x(T_e d_n^2+T_x d_e^2) \end{pmatrix}. \tag{3.4}$$

This representation of $\mathbf{M}$ is so ordered that the 1st, 2nd, and 3rd rows (columns) correspond to e, n, and x, respectively.

Since the general solution of Eq. (3.4) is quite complex, we consider specific cases:

A. Weak Examining ESR Field

This is not an ENDOR situation involving saturation enhancement, but nevertheless is of interest. All terms in Eq. (3.4) containing d_e may now be set equal to zero. One may then either set $\Delta_e=0$ and sweep through ω_n, or alternatively set $\Delta_n=0$ and sweep through ω_e.

(i) Let $\Delta_e=0$. Then,

$$Z''_e = q\omega_e d_e T_e \times[T_x^2\Delta_n^2+1+T_e T_x d_n^2]/[T_x^2\Delta_n^2+(1+T_e T_x d_n^2)^2]. \tag{3.5}$$

The presence of a finite d_n is seen to deenhance the resonant ESR signal, and a maximum deenhancement occurs for $\Delta_n=0$. The cause of the deenhancement is readily seen by examining Case (ii).

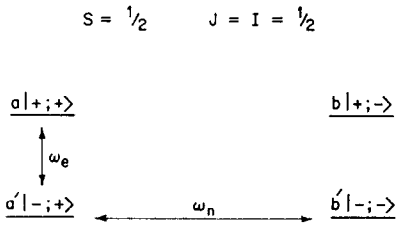

(ii) Let $\Delta_n=0$. Then

$$Z''_e = q\omega_e d_e T_e/[1+T_e^2\Delta_e^2+T_e T_x d_n^2(1-\xi_e)] \tag{3.6a}$$

with

$$\xi_e=(T_e+T_x)^2\Delta_e^2/(1+T_x^2\Delta_e^2+T_e T_x d_n^2) \tag{3.6b}$$

The denominator in Eq. (3.6a) can have more than one minimum. Thus, differentiating Z''_e with respect to Δ_e and setting it equal to zero, we get extrema for $\Delta_e=0$, and

$$\Delta_e^2 = yT_x^{-2}[d_n(T_e+T_x)(T_x/T_e)^{1/2}-y] \tag{3.7a}$$

where

$$y=(1+T_e T_x d_n^2)^{1/2}. \tag{3.7b}$$

One finds from Eq. (3.7) a critical value of d_n,

$$d_n^{\text{crit}} = \pm T_x^{-1}(2+T_x/T_e)^{-1/2} \xrightarrow{T_x \to T_e} \pm 1/\sqrt{3}T_e. \tag{3.7c}$$

For $d_n > d_n^{(\text{crit})}$, there are two peaks in the ESR experiment given by Eq. (3.7a), but for $d_n < d_n^{(\text{crit})}$ there is only one peak at $\Delta_e=0$. When $T_e T_x d_n^2 \gg 1$ we have: $\Delta_e=\pm d_n$, and this becomes a useful method for measuring B_n. In Fig. 3, computer simulations based on the solution of Eqs. (3.4) and (2.4a) (for different values of $d_n^2 T_e T_x$) are given and show this effect. The detailed choice of the relaxation terms, i.e,, the linewidths and saturation parameters, is discussed in Appendix A. Once B_n has been calibrated, it could be possible to determine T_x from Eq. (3.7c). This coherence splitting of the ESR spectrum by a strong NMR field is closely analogous to a well-known NMR double-resonance effect.[9]

[8] There is some simplification on notation here over that in Ref. 3 by specifically labeling the electronic $-e$, nuclear $-n$, and double quantum $-x$ terms. Thus we have $T_e = T_{a'a}$, $T_n = T_{b'a'}$, $T_x = T_{b'a}$, etc.

[9] R. Freeman and W. A. Anderson, J. Chem. Phys. **37**, 2053 (1962).

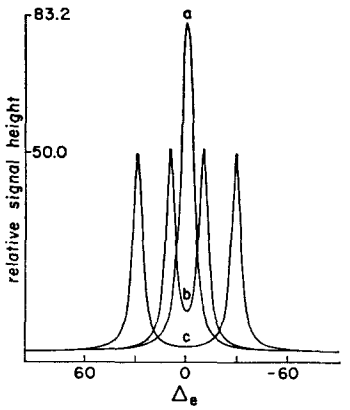

FIG. 3. The effect of a resonant NMR field in splitting one hyperfine component of the ESR spectrum for a radical with $S=\frac{1}{2}$, $I=\frac{1}{2}$. Here $d_e^2T_e\Omega_e\ll 1$. Line shapes a, b, and c are, respectively, for $d_n^2T_eT_x$ equals 0.202, 9.0, 81. The relative signal height is normalized to the simple ESR signal taken as unity. $T_c^{-1}=T_x^{-1}=3.3$ units.

B. Very Weak NMR Field

All terms in Eq. (3.4) containing d_n may be set equal to zero. Z''_e becomes an ordinary saturated Lorentzian and is unaffected by d_n.

C. Strong ESR Field but Weaker NMR Field

Here we require that d_n is still strong enough to saturate the NMR, or

$$T_n\Omega_n d_n^2 \gtrsim 1 \tag{3.8}$$

so the induced relaxation effects of the NMR field on the ESR are *not* negligible. We further require that

$$d_e \gg d_n \tag{3.9}$$

such that the inequality given by Eq. (3.1) holds, but the inequality Eq. (3.2) is, in fact, *reversed*. That is, we expect a coherence splitting of Z''_n by d_e, but *no* splitting of Z''_e by d_n. The coherence splitting on Z''_n could then be observed via an ENDOR enhancement technique when Eq. (3.8) is valid. Such a procedure could, in principle, be a useful method of calibrating B_e (or d_e) (see Sec. V). This coherence effect is illustrated in Fig. 4 wherein are shown computer simulations [based on Eq. (3.4)] of the ENDOR signals (as Δ_n is varied) for values of the parameters chosen to try to optimize the effect. It is found that the desired splitting is obtained in a region where ENDOR enhancements are only 1% or less of the maximum obtainable pure ESR signal (i.e., for $d_e^2T_e\Omega_e=1$). That is, one is seriously saturating the ESR signal in the region where d_e is effectively splitting the NMR resonance. Clearly, relative changes in relaxation parameters can affect this picture, but an increase in the ratio T_n/T_e over that used in Fig. 4 is found to further mask this effect. The value of $T_n/T_e=1$ used in Fig. 4 is, in fact, the realistic lower limit for this ratio (see Appendix A).

It should be noted that the incipient coherence effect due to d_e is a broadening of the ENDOR line, and this incipient effect is more easily achieved than the actual splitting.

IV. EFFECTS OF Rf COHERENCE ON THE NUCLEAR LEVELS IN ENDOR

In this section we assume that Eqs. (3.1)–(3.3) (properly generalized) are fulfilled, so that it is possible to neglect electron-nuclear coherence effects of the type discussed in Sec. III. Then the simplest case of interest is for $S=\frac{1}{2}$, $I=1$ and is given by Fig. 1. There is still one two-quantum transition Z_c involving coherence between nuclear levels. This double quantum transition is included in Eqs. (2.4) as applied to the present case. It is useful to take $\mathbf{M}$ and transform it to a basis involving the sum and difference terms:

$$(1/\sqrt{2})\,(Z_1 \pm Z_2) \equiv Z_\pm \tag{4.1}$$

by means of an orthogonal transformation $\mathbf{UMU}^{-1}$, where

$$\mathbf{U}=\mathbf{U}^{-1}=\begin{pmatrix} 1 & 0 & 0 & 0 \\ 0 & 1/\sqrt{2} & 1/\sqrt{2} & 0 \\ 0 & 1/\sqrt{2} & -1/\sqrt{2} & 0 \\ 0 & 0 & 0 & 1 \end{pmatrix}. \tag{4.2}$$

This transformation has no effect on Z_e and Z_c (where now Z_e represents either of the three allowed ESR

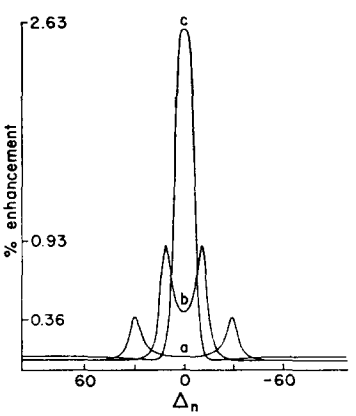

FIG. 4. The effect of coherence splitting of the NMR for a radical with $S=\frac{1}{2}$, $I=\frac{1}{2}$ by a strong resonant ESR field. It is observed indirectly via the ENDOR enhancement of the ESR signal. Here $d_n^2T_n\Omega_n=1.0$, $T_e=T_x=T_n=0.3$ reciprocal units and $b=1$ (see Appendix A). The line shapes a, b, and c correspond to value for d_e of 5, 12, 30 units respectively. The percent enhancement for each case is given relative to the magnitude of the maximum obtainable ESR signal in the absence of an ENDOR effect.

transitions). Thus

$$\mathbf{UMU}^{-1}=\tilde{\mathbf{M}}=\begin{pmatrix} 1+T_e^2\Delta_e^2+T_eS_e & (1/\sqrt{2})T_eS_{e,+} & (1/\sqrt{2})T_eS_{e,-} & 0 \\ (1/\sqrt{2})T_+S_{e,+} & 1+T^2{}_+\Delta_n^2+T_+S_+ & 0 & 0 \\ (1/\sqrt{2}T_-S_{e,-} & 0 & 1+T_-{}^2\Delta_n^2+T_-S_-+2d_n^2T_cT_- & \sqrt{2}(T_-+2T_c)T_-\Delta_nd_n \\ 0 & 0 & \sqrt{2}T_c(T_-+2T_c)\Delta_nd_n & 1+4T_c^2\Delta_n^2+2T_cT_-d_n^2 \end{pmatrix}, \tag{4.3}$$

and

$$\tilde{\mathbf{M}}\mathbf{UZ}=\mathbf{U}(-\mathbf{R}^{-1})\mathbf{Q}, \tag{4.4a}$$

with

$$\mathbf{UZ}''=\begin{pmatrix} Z''_e \\ Z''_+ \\ Z''_- \\ Z''_c \end{pmatrix} \tag{4.4b}$$

$$\mathbf{U}(-\mathbf{R})^{-1}\mathbf{Q}\cong q\omega_eT_e\begin{pmatrix} 1 \\ 0 \\ 0 \\ 0 \end{pmatrix}. \tag{4.4c}$$

In Eq. (4.3), $S_{e,\pm}=S_{e,1}\pm S_{e,2}$ and $T_\pm=T_1\pm|T_{1,2}|$[10]. Also $q=\hbar/kT$. We note there is no coupling between the symmetric mode Z_+ and either Z_- or Z_c, but Z_- and Z_c do couple as a result of coherence terms. Now physically Z''_+ represents the net rf induced absorption from State f to State b, for which an equation similar to Eq. (2.7) may be written. This is the *only* mode that is detected in a conventional NMR experiment. That is, the power absorbed in such an experiment may be calculated from[3,11]

$$\begin{aligned} P&=-(i/2)\mathfrak{V}\hbar\gamma_n\omega_nB_n \\ &\quad\times\mathrm{Tr}\{\sigma(t)[I_+\exp(-i\omega_nt)-I_-\exp(+i\omega_nt)]\} \\ &=2\sqrt{2}\mathfrak{V}\hbar\omega_nd_nZ''_+. \end{aligned} \tag{4.5}$$

Equation 4.5 expresses the well-known result that the only effect of the coherence of the rf field on a simple nuclear resonance experiment appears as a saturation effect with no frequency shifts. The difference mode Z''_- is not detected in NMR, but *does* affect the ENDOR spectrum by means of its coupling to Z''_e via a finite $S_{e,-}$. Now Z''_- represents the net rf induced absorption from States b and f to State d, [i.e., it is proportional to $(\sigma_f+\sigma_b-2\sigma_d)$], and it does not correspond to any net energy absorption.[12] The significance of the two-quantum term Z_c is closely related to that of Z_-. Thus, from Eq. (2.3a) as applied to this problem, one obtains:

$$Z_c=-\sqrt{2}d_nZ_-/[2\Delta_n-(i/T_c)], \tag{4.6a}$$

so Z_c also does not correspond to any net energy absorption. When $\Delta_n=0$, we have:

$$Z''_c=Z'_+=Z'_-=0, \tag{4.6b}$$

and

$$Z'_c=\sqrt{2}d_nT_cZ''_-, \tag{4.6c}$$

and at resonance there is only a dispersive mode at frequency $2\omega_n$.

One could diagonalize the lower right hand 2×2 component of $\mathbf{M}$ given by Eq. (4.3) to obtain the normal modes of the coupled Z''_- and Z''_c transitions. But, since the transformation matrix itself is a function of Δ_n, and it is Z''_- which directly affects the ENDOR line shapes, this is not a very useful procedure.[13]

The ESR absorption Z''_e, that is obtained from Eqs. (4.3) and (4.4) is given by

$$Z''_e=q\omega_ed_eT_e/[1+(\Delta_eT_e)^2+(\Omega_e-\xi_e)T_ed_e^2], \tag{4.7}$$

where

$$\begin{aligned} \xi_e&=(\tfrac{1}{2}T_+\Omega_{e,+}{}^2d_n^2)/(1+T_+{}^2\Delta_n{}^2+T_+\Omega_+d_n{}^2) \\ &\quad+\left(\tfrac{1}{2}T_-\Omega_{e,-}{}^2d_n{}^2M_{xx}\Big/\begin{vmatrix} M_{--} & M_{-x} \\ M_{x-} & M_{xx} \end{vmatrix}\right), \end{aligned} \tag{4.8}$$

[10] Here

$$T_1=T_2=-R_{1,1}(R^2{}_{1,1}-R^2{}_{1,2})^{-1}$$

and

$$T_{1,2}=-R_{1,2}(R^2{}_{1,1}-R^2{}_{1,2})^{-1}$$

and the elements of $\mathbf{R}$ may be obtained from Eqs. (A4) and (A5).

[11] A. Abragam, *The Principles of Nuclear Magnetism* (Oxford University Press, London, 1961), p. 48.

[12] Another reason why Z_- would be unimportant in pure NMR is that one expects: $(\sigma_e-\sigma_c)-(\sigma_c-\sigma_a)=0$, so there is no net population difference for this transition mode. However, in ENDOR, because of the presence of a saturating ESR field the electron-spin Boltzmann factor in $\mathbf{Q}$ far outweighs the nuclear-spin factor and this equation is no longer true.

[13] The condition given by Eq. (4.19) in I for the neglect of coherence effects in this situation may be seen to follow from the eigenvalues of such a diagonalization. But since the transformation matrix is neglected, it is inappropriate for the present problem. Actually, if we let $T_-\sim T_c$, then when $\Omega_-/T_c\geq4.5$ (which is usually the case) there is no departure of the exact resonant frequency of the normal mode components from $\Delta_n=0$. A simple diagonalization of $\mathbf{K}$ yields normal modes that are identical to this case given $\Omega_-/T_c=0$,i.e., extrema at $\Delta_n=0$ and $\Delta_n=\pm d_n$.

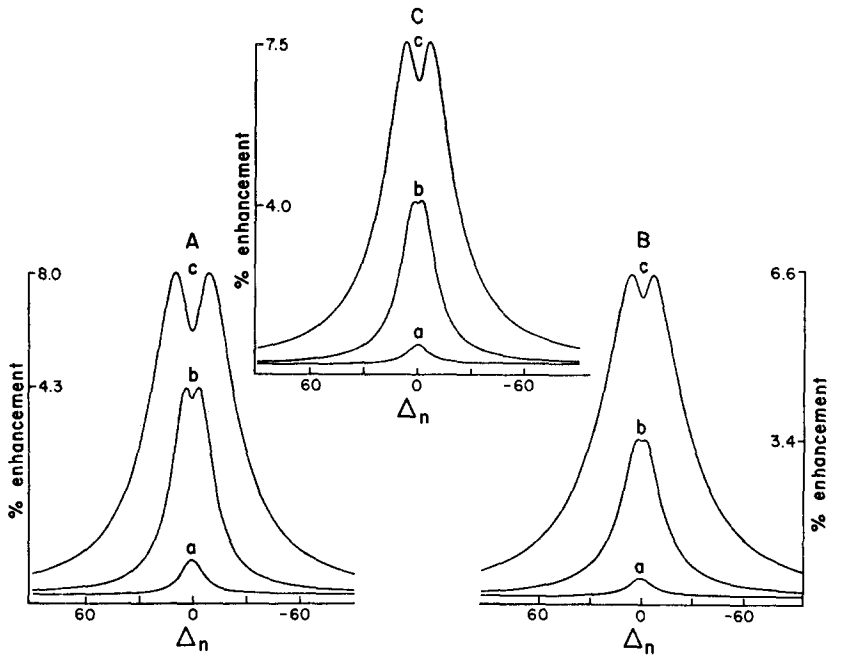

FIG. 5. The ENDOR line shape when the $M_J=0$ ESR line is saturated. In (A) $J=1$; (B) $J=2$; (C) the composite line from four equivalent spins of $I=\frac{1}{2}$ obtained from A and B properly weighted. All cases correspond to $b=1$, $T_e^{-1}=53.3$ units (see Appendix A). In (A) $d_e=10.4$. In each, the line shapes a, b, and c correspond to $d_n=1$, 4 and 10 units, respectively. Each signal height is given relative to the magnitude of the original saturated ESR line.

where M_{ii} refer to the elements of **M** given in Eq. (4.3) and the denominator in the second term on the right-hand side is a 2×2 determinant. One may easily find that the extrema for the second term in Eq. (4.8), given the reasonable condition $T_c\sim T_-\equiv T$, occur at

$$\Delta_n=0 \quad \text{and} \quad \Delta_n^2=\tfrac{1}{4}[3d_n(2X)^{1/2}-X], \qquad (4.9)$$

where

$$X=T^{-2}(1+2T^2d_n^2). \qquad (4.9')$$

For $d_nT\gg1$, we have $\Delta_n=\pm d_n$ or two peaks separated by $2d_n$.[14] Also there is a critical value $d_n^{(\text{crit})}=(4T)^{-1}$ below which there is no splitting but only a single line centered at $\Delta_n=0$. The first term on the right-hand side in Eq. (4.8) is just a single (saturated) Lorentzian centered at $\Delta_n=0$. Now the $\Omega_{e,\pm}$ in Eq. (4.8) indicates the effectiveness of these two nuclear-spin modes in decreasing the ESR saturation parameter. The results depend markedly upon whether the center ESR line or one of the outside ESR lines is being saturated, and this may be understood in terms of simple symmetry considerations. Consider first the center ESR line (Fig. 1). If we neglect nuclear-spin Boltzmann factors and any linear dependence of lattice-induced spin-relaxation processes on M_I, then $Z''_{db}=Z''_1$ and $Z''_{df}=-Z''_2$ are seen to have identical effects on Z''_{0e}, i.e., they enhance symmetrically equivalent paths of relaxation. Furthermore the Z''_{0e} transition will have identical (Overhauser) effects on each of these nuclear spin transitions so that $Z''_1=-Z''_2$. (Note that the minus corresponds to the transition arrow with a reversed direction.) Thus $Z''_+=0$, (i.e., one does not get any Overhauser enhancement of the NMR signal by saturating Z''_{0e}), and this mode does not contribute to the ENDOR enhancement of Z''_{0e}. In terms of Eqs. (4.3)–(4.4), this result is obtained because $\Omega_{0e,1}=-\Omega_{0e,2}$, so $\Omega_{0e,+}=0$. Therefore, only Z''_- can contribute to Z''_{0e} (and concurrently the Z''_- mode experiences an Overhauser enhancement), and Z''_- should demonstrate a frequency splitting for large values of d_n. When Z''_{+e} is being saturated, no such symmetry exists, so both nuclear spin modes may contribute, but in the region of appreciable ENDOR enchancements (i.e., $b\approx1$) one finds that $\Omega_{+e,+}>\Omega_{+e,-}$. The computer simulations of the ENDOR line shapes, Figs. 5A–7A, for chosen values of the relaxation parameters (see Appendix) demonstrate that the composite effect obtained for Z''_{+e} leads just to a single peak even for very large d_n, where a definite splitting for Z''_{0e} is obtained.

$I=2$

In a manner similar to the $I=1$ case, one may obtain line shapes for various d_n for the five-line $I=2$ case. Here there are 4 single, 3 double, 2 triple, and 1 quadruple nuclear-spin quantum transitions. Again, it is found that for $M_I=0$ the ENDOR line doubles as d_n increases [cf. Fig. 5(B)]. While the $M_I=\pm2$ lines show no qualitative change [cf. Fig. 7(B)] in shape, the $M_I=\pm1$ lines exhibit the appearance of two shoulders symmetrically placed about the center as d_n is increased [cf. Fig. 6(B)]. These shoulders become more pronounced with further increase in d_n. Simulations neglecting effects from multiple quantum transitions greater than two are qualitatively the same as Figs. 5(B)–7(B), but there are some quantitative differences.

The four equivalent spins of $I=\frac{1}{2}$ case (here $J=2$)

[14] It is interesting to note that this asymptotic limit is approached from the high side, i.e., for $d_nT\gg1$, $\Delta_n=\pm d_n(1+|\epsilon|)$ with $\epsilon\to0$. The location of extrema is also affected by the relative values of T_e and T_-. Estimates show, however, that when $T_e/T_-\approx1.1$, a decrease in separation of the extrema of only about 1.5% is expected.

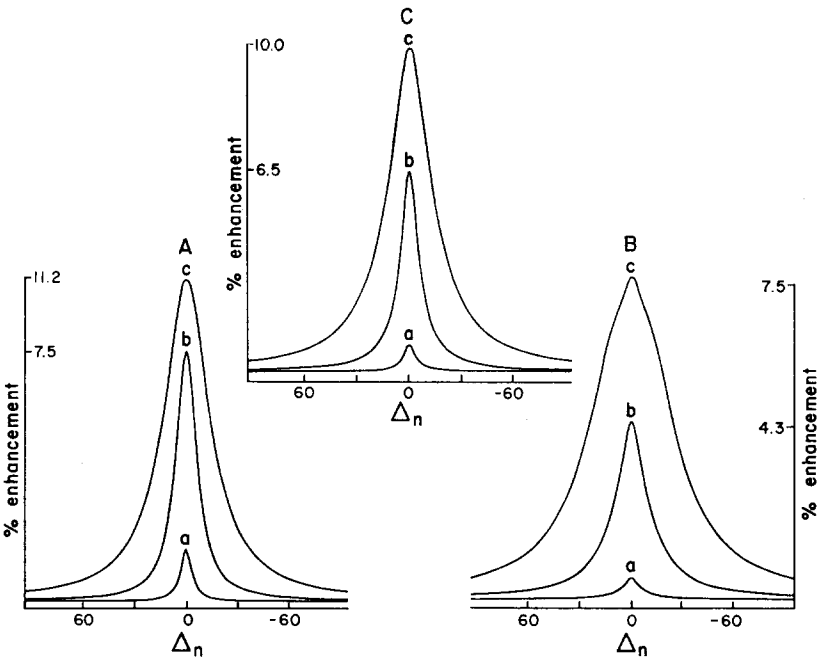

FIG. 6. The ENDOR line shape when the $M_J=\pm 1$ ESR line is saturated. In (A) $J=1$; (B) $J=2$; and (C) the composite line from four equivalent spins of $I=\frac{1}{2}$ obtained from (A) and (B) properly weighted. All cases correspond to $b=1$, $T_e^{-1}=53.3$ units (see Appendix A). In (A) $d_e=10.4$. In each, the line shapes a, b, and c correspond to $d_n=1$, 4, and 10 units, respectively. Each signal height is given relative to the magnitude of the original saturated ESR line.

may be obtained by superposing the $I=1$ case with degeneracy 3 and the $I=2$ case with degeneracy 1. The $M_J=\pm 2$ line is the same as for the $I=2$ case, but the $M_J=\pm 1$, 0 lines are dominated by the $I=1$ components. These are given in Figs. 5(C)–7(C). The relative contribution from the $I=2$ component is enhanced as the parameter b is reduced from the present assumed value of unity. This is because the optimum enhancement region depends inversely on $I(I+1)$. (cf. Appendix A.)

$I=\frac{3}{2}$ and $\frac{5}{2}$

Detailed analysis shows that the $I=\frac{3}{2}$ case behaves qualitatively like the $I=1$ case. That is, there is a similarity between the $M=\pm\frac{3}{2}$, $I=\frac{3}{2}$ and $M=\pm 1$, $I=1$ lines and also between the $M=\pm\frac{1}{2}$, $I=\frac{3}{2}$ and $M=0$, $I=1$ lines. The $I=\frac{5}{2}$ case is similar to that for $I=2$ with the $M=\pm\frac{1}{2}$ lines showing a splitting, the $M=\pm\frac{3}{2}$ lines develop shoulders, and the $M=\pm\frac{5}{2}$ lines only broaden.

V. EXPERIMENTAL RESULTS AND DISCUSSION

The first free radical studied by ENDOR,[1a] Coppinger's radical [Fig. 8(a)], gives ENDOR signal heights as high or higher than any radicals observed subsequently by this technique. The spectrum may be studied over a wide range of temperatures in low dielectric loss solvents. It saturates relatively easily compared with other free radicals in solution, implying that the spin packet width is less. Coppinger's radical is a good system for ENDOR and for this reason our most detailed experimental studies of coherence effects have been performed on it. The samples used had a concentration of about $3\times 10^{-4}M$ in n-heptane and were studied at −85°C.

The ESR spectrum shows two quintets split by coupling to the central (methylenyl) proton, the quintets arising from the four ring protons. The 36 tertiary-butyl protons are weakly coupled and give rise to an inhomogeneous broadening of each of the lines of the spectrum. In the ENDOR experiments described here, the free proton frequency was about 13.57 MHz. The methylenyl coupling is $A=15.59$ MHz, giving rise to ENDOR lines at 21.37 and 5.77 MHz. The ring proton coupling is 3.87 MHz, giving rise to ENDOR lines from these four protons at 15.51 and 11.63 MHz.

A. Strong ESR Field but Weaker NMR Field

In Fig. 9 the ENDOR line from the central (methylenyl) proton is shown as a function of microwave power. The line is observed to broaden and split as this power is increased. The amplitude of the microwave field B_1 was measured using the technique of the perturbing metal sphere[15] (see Appendix B). This technique makes no assumption about the microwave field distribution. The maximum value of B_1 in the rotating frame with 1.5 mW of incident power was 0.044± .01 G. At 27 mW, this corresponds to 0.187 G. Using the gyromagnetic ratio of the electron, 2.80 MHz per G, one might expect a splitting of 523 kHz. The observed splitting in Fig. 9 is 470 kHz, which agrees with the predicted value within experimental error. Actually, this splitting is expected to be altered somewhat by the fact that a line sample was employed which extends through the microwave cavity and as a result experiences a nonuniform microwave field. However, the

[15] E. L. Gintzon, *Microwave Measurements* (McGraw-Hill Book Co., New York, 1957), p. 448. We wish to thank Mr. R. G. Kooser for deriving the results in this Appendix.

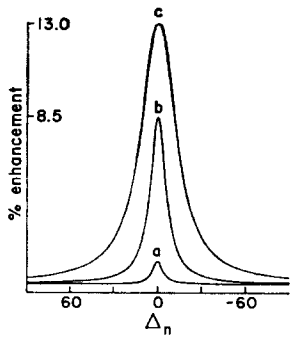

FIG. 7. The ENDOR line shape when the $M_J=\pm 2$, $J=2$ ESR line is saturated. Here $b=1$, $T_e^{-1}=53.3$ units (see Appendix A). The line shapes a, b, and c correspond to $d_n=1$, 4, and 10 units, respectively. Each signal height is given relative to the magnitude of the original saturated ESR line.

central portion of the sample experiences the maximum field modulation amplitude so that this portion tends to dominate. That portion of the sample which is in a weaker microwave field gives rise to a signal of smaller splitting. Thus the over-all effect of the nonuniform field would be to broaden the lines and reduce the average splitting from that expected from the maximum value of B_1.

In Ref. 1b it is stated that the maximum observed ENDOR signal intensity which could be obtained from Coppinger's radical is 10% of the ESR signal intensity. Using this result, the ENDOR line obtained at 27 mW is about 1% of the ESR signal intensity.

The shape of the split line was extremely dependent on the portion of the line ($M=0$ of the high field quintet), where the ESR resonant condition was held. A position was empirically selected which gave the most nearly symmetrical line. The lack of symmetry arises because one adjusts to a peak of the first derivative of the line rather than the line center. (This effect has been reproduced in computer simulations.)

Essential agreement with the theory of Sec. III is apparent. To our knowledge this variation of the tickling experiment,[9] where the split line is observed via the ENDOR mechanism as a change in the signal induced by the rf source actually causing the splitting, has not previously been observed in double-resonance experiments.

B. Splitting of the ENDOR Lines by a Strong NMR Field

The ENDOR equipment used for the initial studies[1] unfortunately had no provision for varying the nuclear rf power. The signal from the four ring protons showed a doublet, suggesting that the molecule was bent and that the four protons were not equivalent. In a subsequent version of the equipment, provision was made for variation of the nuclear rf power, and the doublet was observed to collapse as the power was reduced.

In Fig. 10 the ENDOR signals from the ring protons and the central proton are shown as a function of nuclear rf power. In this figure all experimental parameters except the rf power were held constant. The magnetic field was adjusted to the center ($M=0$) line of the high field quintet. The ring proton signal broadens and splits with increasing power. A slight broadening of the line from the central proton can be seen, but no splitting is observed.

In Fig. 11 the ENDOR traces are shown for the ring protons with the ESR adjusted to the high-field first-derivative peaks of the high field $M=2$, $M=1$, and $M=0$ lines. Essentially identical results were obtained on the low-field first-derivative peaks of the high field $M=2$, $M=1$, and $M=0$ lines. Careful measurements moving the ESR resonant condition through the $M=0$ ESR line showed no change in observed splitting, only a change in observed ENDOR signal amplitude.

The microwave power incident on the cylindrical TE_{011} cavity was 0.4 mW. This level of microwave power gave good signals; reducing it further resulted in a reduction of the signal amplitude but not the observed splitting. The nuclear rf field amplitude is difficult to measure experimentally, but is of the order of 20 ± 5 G in the rotating frame which could yield splittings as large as 120 ± 30 kHz. [Cf. Eq. (4.9).] On various runs the observed splitting was in the reasonable range of 70 to 90 kHz.

Coherence effects have been seen in the ENDOR spectrum of the triphenylmethyl radical. In this spectrum the ENDOR line from the six equivalent *meta* protons showed a splitting similar to that seen in Coppinger's radical. However, neither the line from the *ortho* nor the line from the 3-*para* protons show a splitting. The ENDOR line width of the six *ortho* protons appears somewhat greater than that of the six *meta* protons, suggesting somewhat shorter relaxation times. The *ortho* and *para* spin densities are about 3 times the *meta* spin density, and the spin density is an important factor in determining relaxation behavior via an END mechanism.[4] Apparently ENDOR linewidths are sufficiently altered to make the splitting not observable. [Cf. Eq. (4.9).]

When performing ENDOR on complicated free radicals it is customary to use a field modulation amplitude which gives the largest obtainable ESR signal height. Often one may use 5–10 G resulting in overmodulation of the EPR spectrum. This does not affect the ENDOR linewidth since these widths are about 150 kHz and, using a gyromagnetic ratio of 4.2 kHz

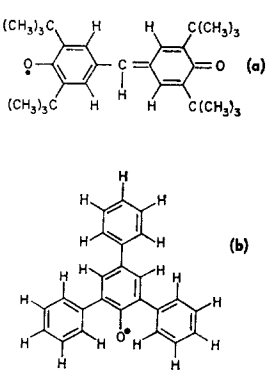

FIG. 8. Molecules exhibiting ENDOR coherence effects: (a) Coppinger's radical; (b) triphenylpheoxyl radical

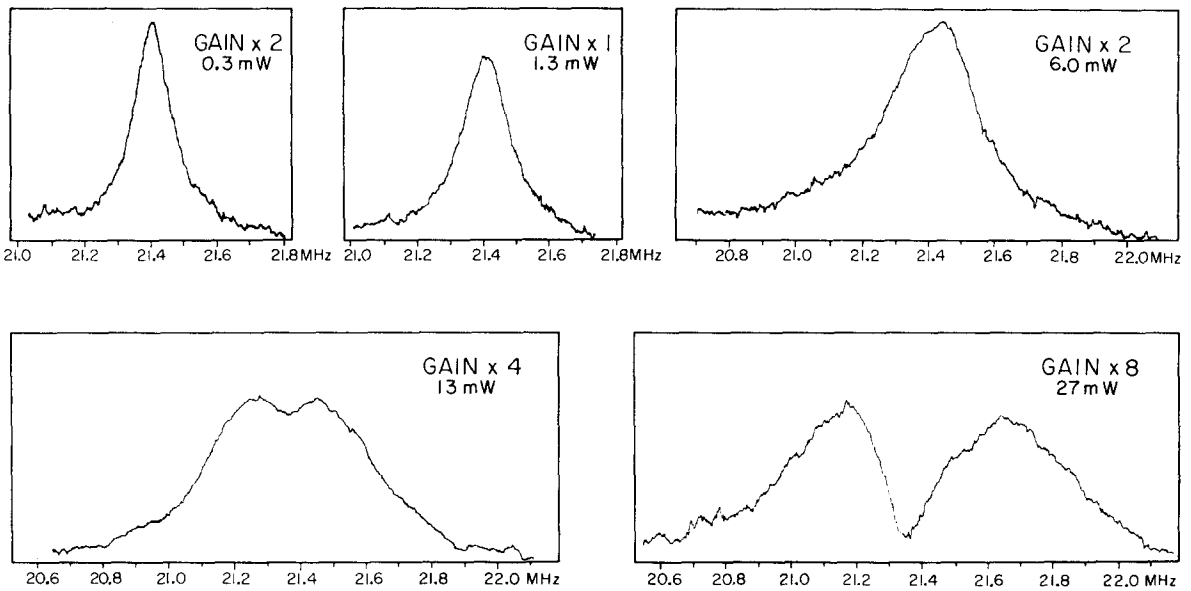

FIG. 9. The ENDOR line from the methylenyl proton of Coppinger's radical as a function of microwave power. The power incident on the cavity is given in milliwatts and the relative recorder gain is indicated.

per G, this amounts to widths of 36 G. This technique was used to obtain the triphenylmethyl spectrum. We emphasize it in order to point out that even under common ENDOR experimental conditions of gross overmodulation, coherence effects are observable.

These experimental results appear to fit the theory of Sec. IV in nearly all details:

1. No effect is observed for a single proton ENDOR Line.

2. The effect is observed most clearly on the $M=0$ lines of the four equivalent protons.

3. For the $M=1$ line there is a suggestion in the observed spectra of a line shape similar to Fig. 6(B). (This would imply a greater contribution of the $I=2$ component of the composite line in Fig. 6(C). As noted in Sec. IV, reducing the parameter b would have such an effect.)

4. No effects are seen for $M=2$.

5. The microwave power level does not affect the observed splittings at moderate saturation, but broadens the ENDOR lines at higher saturation levels making the splitting more difficult to observe. (This is an incipience of the coherence effect discussed theoretically in Sec. IIIC and experimentally in Sec. VA.)

6. The value of the nuclear rf field required to observe these effects is consistent with the formulation.

7. The splitting does not depend on the part of the line where the ESR resonant condition is maintained.

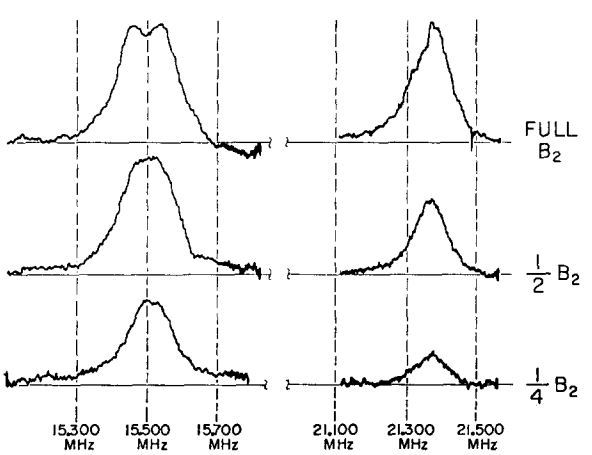

FIG. 10. ENDOR lines from Coppinger's radical as a function of nuclear rf field strength B_2. The $M=0$ ring proton signal is at 15.51 MHz and the methylenyl proton signal is at 21.37MHz. Full B_2 is about 20 G.

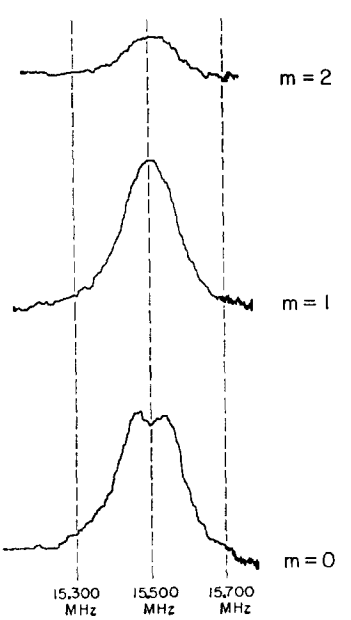

FIG. 11. ENDOR line of the ring protons of Coppinger's radical with the magnetic field adjusted to the $M=0$, 1, and 2 high-field hyperfine lines.

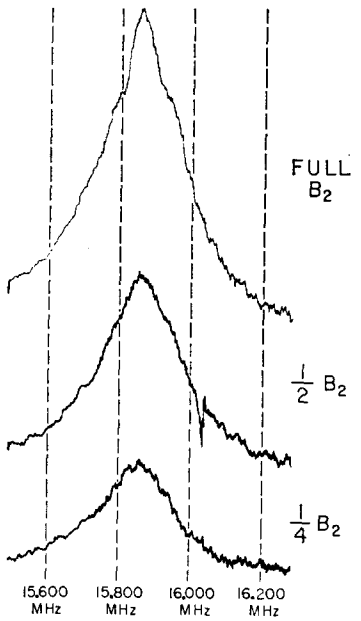

FIG. 12. ENDOR of two nearly degenerate pairs of equivalent protons in the triphenylphenoxyl radical as a function of B_2.

Whether or not these coherence effects are observed appears also to depend critically on the ENDOR linewidth [cf. Eq. (4.9)]. For example, N Coppinger's radical [the radical in Fig. 8(a), but with the central C–H replaced by N] saturates somewhat less easily with microwave power under identical conditions; the ENDOR lines are somewhat broader, and no splitting has been observed.

C. Coherence Effect from nearly Degenerate ENDOR Lines

An effect which we believe is similar to those already presented was found in the ENDOR study of the triphenylphenoxyl radical [Fig. 8(b)], in benzene. Three nearly degenerate lines are found arising from the two ring protons, the two *ortho* protons of the 4-phenyl and the *para* of the 4-phenyl. If the 4-phenyl is completely deuterated, a line is obtained from the ring protons corresponding to a hyperfine coupling of 4.703 MHz. If only the *para* proton is deuterated, a coupling is observed of 4.589 MHz and is the superposition of the line from the *ortho* protons of the 4-phenyl and the ring protons. Thus a coupling of 4.475 MHz was assigned to the 4-phenyl *ortho* protons. The ENDOR signals from this latter sample (deuterated only at the *para* position of the 4-phenyl) as a function of nuclear rf power are shown in Fig. 12. The shoulders on either side of the line obtained at full power are reproducible and real. This behavior was qualitatively independent of microwave power. We suggest that this line shape behavior at high nuclear rf powers is one manifestation of the type of coherence effects under discussion in this paper. The line shape obtained at full power cannot be simulated by superimposing two lines at 4.475 and 4.703 MHz having the line shape noted for the ring protons. However, the almost accidental degeneracy might well permit some significant coherence coupling effect, but this has not been analyzed.

VI. CONCLUSIONS

The importance of the coherence of the radiation fields in a steady-state ENDOR experiment has been demonstrated theoretically and experimentally in the case of two effects peculiar to the ENDOR situation. In particular there is detailed semiquantitative agreement between the experimental observation and theoretical explanation of the coherence effect arising from strong nuclear rf fields, which causes some, but not all, ENDOR lines to split. This good agreement of such a subtle effect affords further support to the idea that the general characteristics of steady-state ENDOR experiments in liquids are properly understood. We note, also, that this coherence effect could have some analytical value. Thus, for example, if a splitting is seen, the ENDOR line must arise from more than one equivalent proton. Also, careful measurements of the splitting as a function of nuclear rf power could lead to its calibration, provided that very strong rf fields are obtainable. However, the effect discussed in Sec. IIIA should accomplish this calibration more simply. The other coherence effect arising from strong microwave fields could also be used for purposes of calibration, and it appears to agree reasonably well with more conventional measurements.

APPENDIX A

The computer simulations in Figs. 3 to 7 are based on an assumption of slow tumbling, i.e., $\omega_e^2\tau_c^2 \gg 1$ which appears to be a favorable condition for obtaining ENDOR enhancements.[3] Under these conditions we may approximate W_e by

$$W_e \cong W_e^G + W_e^{SR} + X, \tag{A1}$$

where

$$W_e^G = 2j^{G_2}(\omega_e) B_0^2 \xrightarrow[\omega_e\tau_c \gg 1]{} \sum_i (g_i - g_s)^2/40\tau_c, \tag{A1'}$$

and

$$W_e^{SR} = \sum_i (g_i - g_e)^2/18\tau_c, \tag{A1''}$$

where g_i is the ith component of the g tensor in its principal axis system, while g_s and g_e are the average g values for the radical and the free electron g values, respectively. The first two terms in Eq. (A1) are the g tensor and spin rotational contributions, and X includes other effects (e.g., intermolecular dipolar terms), so W_e is largely nuclear-spin-independent. ENDOR "active" nuclear spin transitions are due primarily to the effects of the intramolecular anisotropic-electron-nuclear dipolar (END) interaction:

$$W_{(J,M\to J,M\pm1)} = W_n[J(J+1) - M(M\pm1)], \tag{A2}$$

where

$$W_n = \tfrac{1}{2} j^D(0). \tag{A2'}$$

The ESR linewidths are roughly approximated by

$$-R_e=T_e^{-1}\cong T_x^{-1}\cong(8/3)j^{G_2}(0)B_0^2+X' \quad \text{(A3)}$$

and are largely (although not entirely) nuclear-spin-independent. The NMR linewidths are given by

$$-R_{M_a,M_{a'}}=W_n[2J(J+1)+\tfrac{1}{3}(M_a-M_{a'})^2-2M_aM_{a'}]+W_e \quad \text{(A4)}$$

with off-diagonal elements

$$R_{M,M+\rho,M\pm1,M+\rho\pm1}=W_nf(J,\mp M)f[J,\mp(M+\rho)], \quad \text{(A5)}$$

where $\rho=1, 2, 3,\cdots$ for single, double, triple, etc. quantum transitions.

We have set

$$W_e/W_n\equiv b=1 \quad \text{(A6)}$$

in the calculations since this choice yields near optimum ENDOR enchancements,[3] and may, in fact, be realizable in many experiments.[4] (Actually the optimum region is better estimated from $b\cong[J(J+1)]^{-1}$). This condition, Eq. (A6), and Eqs. (A1–A5) fix the relative values of W_e, $W_{J,M\to J,M\pm1}$, hence, all the saturation factors in **S** and the **R** elements given by Eqs. (A4) and (A5). The frequency scale in Figs. 3 to 7 is so chosen that $W_e=W_n$ corresponds to one frequency unit. In comparing Eqs. (A1), (A3), and (A4) we note

$$j^{G_2}(\omega_e)=[1+\omega_e^2\tau_c^2]^{-1}j^{G_2}(0)\gg j^{G_2}(0), \quad \text{(A7)}$$

but the relationship between X and X' will depend upon the nature of any other relaxation effects which may be present. Rather than specifying them in detail we let T_e^{-1}/W_e be an adjustable parameter. If X and X' are neglected in Eqs. (A1) and (A3), then we have for slow tumbling:

$$T_e^{-1}/W_e\cong\tfrac{4}{5}\omega_e^2\tau_c^2\{1+\tfrac{20}{9}[\sum_i(g_i-g_e)^2/\sum_i(g_i-g_s)^2]\}. \quad \text{(A8)}$$

More detailed expressions than those being used here for order of magnitude estimates may be found in Refs. 3, 4, and 6.

APPENDIX B

By the method of perturbing spheres,[15] it is possible to determine reduced microwave E and H field strengths at a position in the cavity by the shift in cavity resonant frequency induced by a small metallic sphere placed at that position. Thus, in a region of zero electric field E, one has

$$H_0^2=[(\nu^2-\nu_0^2)/\nu_0^2](1/2\pi a^3), \quad \text{(B1)}$$

where $\mathbf{H}_0$ is the reduced magnetic field given by:

$$H_0^2=\mu H^2/2U. \quad \text{(B2)}$$

Here ν_0 is the unperturbed cavity resonance frequency, ν, the perturbed cavity resonance frequency, a, the radius of perturbing sphere, **H**, the linearly polarized magnetic field, and U, the average stored energy in the cavity.

By introducing the definition of the unloaded cavity Q,

$$Q_0=2\pi\nu_0U/W,$$

Eq. (B2) may be rewritten as

$$B^2=\mu^2H^2=(Q_0W/\pi\nu_0)\mu H_0^2. \quad \text{(B3)}$$

W is the power lost in the cavity and is equal to the power incident on the cavity when matched. For a perfectly matched cavity,

$$\tfrac{1}{2}Q_0=Q_L=\nu_0/\Delta\nu, \quad \text{(B4)}$$

where Q_L is the loaded Q and $\Delta\nu$ is the full width at half-power of the reflected signal from the cavity. Equations (B1), (B3), and (B4) may be combined to give an expression for $\mathbf{B}_1$, the rotating component of magnetic field:

$$|\mathbf{B}_1|=\tfrac{1}{2}|\mathbf{B}|=\tfrac{1}{2}\{[(\nu^2-\nu_0^2)/\nu_0^2](\mu W/\pi^2\Delta\nu a^3)\}^{1/2}\times10^4 \text{ G}. \quad \text{(B5)}$$

where all the parameters are experimentally measurable and are in mks units with the exception of $|B_1|$ in gauss.